Conception Optimization and CFD Structure Study of Wind Farm Power Generation Based on WTGS-OWC Combined System With Battery Storage Element

Mansour MADACI, Djallel KERDOUN

LGEC laboratory, University Constantine1 ,ALGERIA

, Postal address: Road Ain El-bay Constantine1 University, Constantine Algeria

zoldaioque@gmail.com, kerdjallel@yahoo.fr

‡ Corresponding Author; Mansour MADACI, LOTS212 LOGTS N°168 Ain Smara, Tel: +213558033065,

,zoldaioque@gmail.com

Received: 04.08.2016- Accepted:25.09.2016

Abstract- In this paper, a deep study and optimization process for wind farm generation system based on full solar, wind and OWC chamber structure for wave energy harvesting with battery storage system element, a combined WTGS (wind turbine generation system) with OWC (oscillating water column chamber) hybrid generation system has been proposed for an offshore generation farms for power lifting, an FEM (finite element modeling) structure study has been applied to a novel proposition using double orifice chamber structure with form optimization for the maximization of the harvested power, from another side for this latter a CFD (Computational fluid dynamics) simulator software module was used for the study of the pneumatic power evolution through the structure. A novel wave generation method was applied to a 1:30 mechanical prototype was proposed for this purpose to get an oscillated wave model through the RWMD method (Real Wave Model Simulator) instead of using an ordinary sin wave generator on the experimental bank to make the waves the closest possible to the real sea waves. An experimental energy management system has been implemented for the battery storage energy control using two phase interleaved electronic system for the battery charging process between this latter and the full system. A DC-DC converter for the management of the global power system flowing to the grid has been studied for this purpose.

Keywords- (OWC) Oscillating Conversion Chamber device, FEM Finite Element Method, CFD Computational fluid dynamics, RWMS method Real Wave Model Simulator, wind turbine combined generation system, Solar energy, Lead acid battery cell, two phase interleaved DC-DC converter.

1. Introduction

The worldwide requirement for the electricity power is expected to be double within the next 20 coming years. The wave energy available in the large oceans is a huge resource that could be exploited to cover the major requirement for the upcoming energy demand. A British study has claimed that 90 million gigawatts of energy are available on the offshore side of the worldwide oceans. Comparing the actual world energy consumption around the 15000 gigawatts, the wind driven waves could cover the expected increase of the energy demand [1]

Besides surface wave energy structure, several technology categories are available oscillating water columns (OWC) [2],[3]., The Land Installed Marine Power Energy Transmitter (LIMPET) [4], point absorbers, Offshore Floating Ocean Energy System (OFOES)[5]. The Multiple Oscillating Water Column (MOWC) [6]. Based on the (OWC), the NEREIDA demonstration project in Mutriku in Spain consisting of 16 kW and 18.5 kW turbines [7], [8]. (MOWC) Muti -resonant Oscillating Water Column principe installed off the South West Coast of India near Trivandrum a 150 kW wave power plant prototype [9]. Land Installed Marine Power Energy Transmitter (LIMPET) on the island of Islay, west coast of Scotland [10].

On this context, the authors investigate the study and the improvement of an offshore system based on OWC structure combined with WTGS and solar systems with battery storage element for power lifting and maximization process.

A double sided orifice structure has been proposed on this work to insure the lift on the harvested energy during the upstream and the downstream phases. The dimension of the orifice has been optimized using CFD simulation module for pneumatic power maximization around the turbine area within the orifice chamber structure.

2. Wind Farm Generation WTGS-OWC Plants System Modelling

The Offshore hybrid system conception of an oscillating water column (OWC) device with wind turbine generation system (WTGS) (figure 1) consists of a wind turbine generation system with a device constructed to convert the ocean incident wave from massive mechanical power to a kinetic airflow power for power harvesting maximization. This latter will convert kinetic power of the waves to a mechanical power through the OWC turbine. The extraction of the electrical power could be done through different possible topologies even by using an IG (induction generators), DFIG (doubly feed induction generators) or SG (synchronous generators)

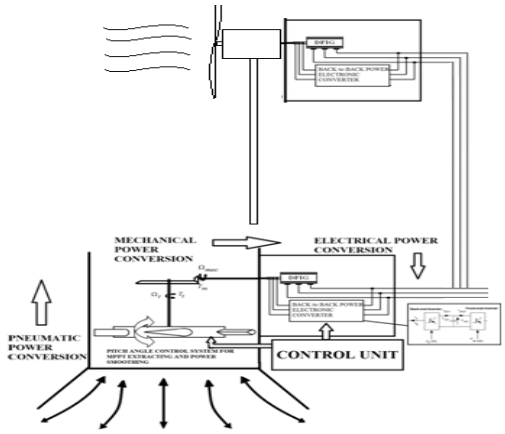

Fig.1. Offshore hybrid system conception of an oscillating water column (OWC) device with wind turbine generation system (WTGS)

2.1 Sea wave model and oscillating wave form propagation

The wave-energy absorption is strongly depended on the sea wave oscillations; the movement of this latter is a time varying oscillatory phenomena. In order to make an adequate wave model, it is necessary to take into account the wave form variation to get an overview on the amount of wave energy available as a function of the wave oscillating frequency.

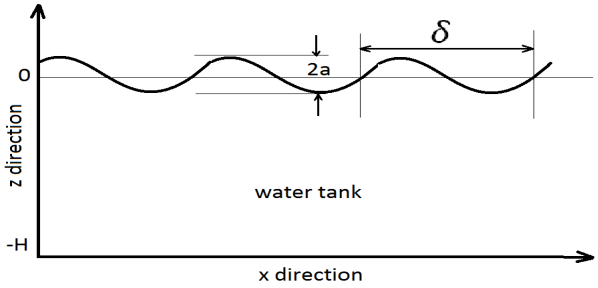

Fig.2. Incident wave propagation on the (X, Z) frame

During the diffrent study steps process of this work, the water is considered as an incompressible fluid, with a density ρ. In the rest, the free surface separation air-water on the limit is taken as an origin for the vertical axis. In the presence of swell the surface oscillations could be represented by the following function

$$h(x,t) = a.\cos\left[j(wt-kx)\right] = a\,\mathrm{Re}\left\{\exp\left[j(wt-kx)\right]\right\} \quad (1)$$

This determines the contact free surface air-water where: from figure 2 and the equation (1): a presents the wave amplitude, $k = 2\pi/\delta$ and δ is the wave length.

From another side, the velocity of a particle from the fluid on the bidirectional frame (x, z) as an origin for the fluid movement on the same frame with (x_0, z_0) as an initial position of the particle on the time (t=0) and on a complex notation:

$$v = \left[v_x(h)e_x + v_z(h)e_z\right]\left\{\exp\left[j(wt-kx)\right]\right\} \quad (2)$$

v_x , v_z present the fluid movement velocity along the x and z direction respectively.

The pressure on this point could be given with

$$p = p_0 - \rho gh + p_1(h)\exp\left[j(wt-kx)\right] \quad (3)$$

The initial conditions with the absence of swell the previous equation became:

$$p = p_0 - \rho gh \quad (4)$$

In the case of incompressible fluid $\rho = Constant$ $div v = 0$

$$\frac{Dv}{Dt} = g - \frac{1}{\rho}grad\,p \quad (5)$$

So the particle's velocity on the (x, z) directions respectively will be:

$$\frac{Dv_x}{Dt} = -\frac{1}{\rho}\frac{\partial}{\partial x}\left\{p_1(h)\exp\left[j(wt-kz)\right]\right\} \quad (6)$$

$$\frac{Dv_z}{Dt} = -\frac{1}{\rho}\frac{\partial}{\partial z}\left\{p_1(h)\exp\left[j(wt-kz)\right]\right\} \quad (7)$$

The free surface's profile is given by

$$h(x,t) = a\,\mathrm{Re}\left\{\exp\left[j(wt-kx)\right]\right\} \quad (8)$$

The velocity of an elementary particle moves on the z direction for a given point $v_z(h=-H)$ belongs to the deep down of the tank level is equal to zero.

To avoid the complex equations the profile will be:

$$h(x,t) = a\left\{\exp\left[j(wt-kx)\right]\right\} \quad (9)$$

From another side the particle velocity with $v_z(h=-H)=0$ gives:

$$\frac{Dv_x}{Dt} \approx \frac{\partial v_x}{\partial x} = jwv_x(h)\exp\left[j(wt-kx)\right]$$

$$= \frac{jk}{\rho}p_1(h)\exp\left[j(wt-kz)\right] \quad (10)$$

$$v_x(h) = \frac{k}{\rho w}p_1(h) \quad (11)$$

$$\frac{Dv_z}{Dt} \approx \frac{\partial v_z}{\partial x} = jwv_z(h)\exp\left[j(wt-kx)\right] = -\frac{1}{\rho}\frac{dp_1(h)}{dz}\exp\left[j(wt-kx)\right] \quad (12)$$

$$v_z(h) = \frac{j}{\rho w}\frac{dp_1(h)}{dz} - jkv_x(h) + \frac{dv_z(h)}{dz} = 0 \quad (13)$$

$$\frac{d^2p_1(h)}{dz^2} - k^2p_1 = 0 \quad (14)$$

$$p_1(h) = A\exp(kh) + B\exp(-kh) \quad (15)$$

$$v_x = \frac{k}{\rho w}\left[A\exp(kh) + B\exp(-kh)\right] \quad (16)$$

$$v_z = \frac{jk}{\rho w}\left[A\exp(kh) + B\exp(-kh)\right] \quad (17)$$

The effect of the deep on the wave oscillations for the power could be expressed by replacing $v_z(h=-H\rightarrow-\infty)=0$ For this $B=0$. The previous equations could be written as follow to be used for the extraction of a particle position belongs to the fluid on the same frame (x, z)

$$p_1(h) = A\exp(kh) \quad (18)$$

$$v_x = \frac{k}{\rho w}\left[A\exp(kh)\right] \quad (19)$$

$$v_z = \frac{jk}{\rho w}\left[A\exp(kh)\right] \quad (20)$$

The position on this case:

$$\frac{\partial x}{\partial x} = \frac{k}{\rho w}A\exp(kh)\exp\left[j(wt-kx)\right] \quad (21)$$

$$\frac{\partial z}{\partial x} = \frac{jk}{\rho w}A\exp(kh)\exp\left[j(wt-kx)\right] \quad (22)$$

Since for the initial conditions

$$h(x,t) = a\cos\left[j(wt-kx)\right] = \frac{k}{\rho w}A\exp(kh)\cos\left[j(wt-kx)\right] \quad (23)$$

$$h(x,t) = \tfrac{k}{\rho}Acos[j(wt-kx)] \quad (24)$$

$$kh = \tfrac{2\pi}{\delta}h = \tfrac{2\pi}{\delta}a \approx 0 \rightarrow A = \tfrac{\rho w^2 a}{k} \quad (25)$$

On the free surface separation air-water on the limit which was taken as an original to the vertical frame:

$$p_1 = p_0 - \rho gh + \frac{\rho w^2 a}{k}\exp(kh)\cos(wt-kx) \quad (26)$$

$$h(x,t) = a\cos\left[j(wt-kx)\right] = \frac{\rho w^2 a}{k}\exp(kh)\cos(wt-kx) \quad (27)$$

For $\rho = 1$

$$h(x,t) = \frac{w^2 a}{gk}\cos(wt-kx) \quad (28)$$

2.2 Sea OWC Capture Chamber

The first conversion on the power train for an OWC conversion system is restricted by the low conversion ratio during converting the sea wave energy to pneumatic energy. In this context, it is necessary to focus on the improvement of the structure and the design of the OWC converting chamber to increase the efficiency of the system, i.e., chamber design, the electrical system control topology applied to the turbine and the generator.

The different levels on the conversion train need to be analyzed to improve the overall system efficiency. For this purpose, different cases with various test conditions were done to choose the most convenient design for an OWC wave conversion chamber which allows the extraction of the maximum power from the oscillating wave with high

pneumatic energy conversion ratio. As the figure (3.a) and figure (4.a) illustrate the effect of throat expansion angle parameter on the flow stream through the turbine placement area. The evolution of a 12m/s upstream has been boosted from 32m/s (figure 3.b) to 48m/s (figure 4.b).

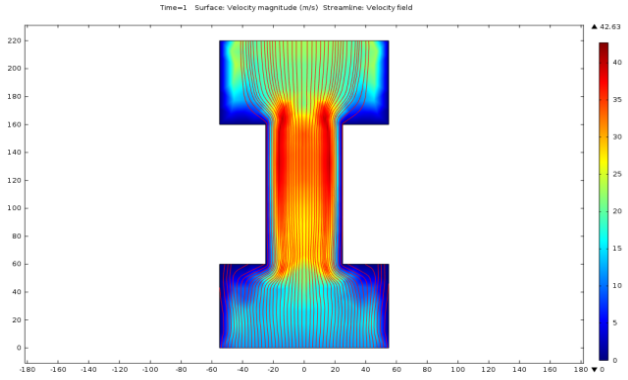

(a)

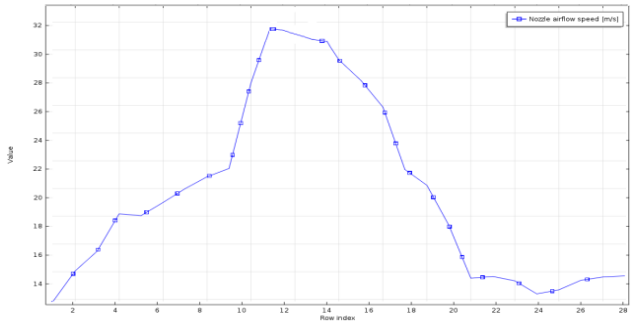

(b)

Fig.3. (a) Orifice shape vertical OWC chamber,(b) inflow evolution along the chamber.

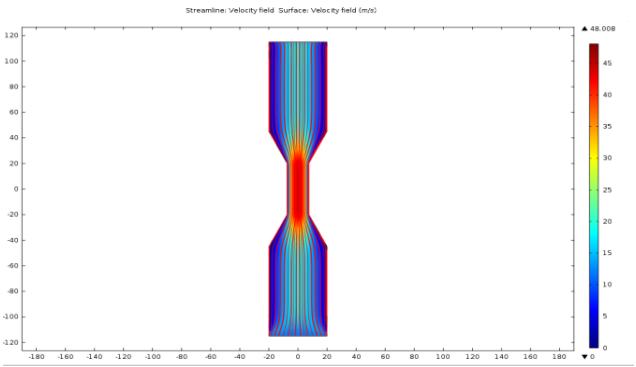

(a)

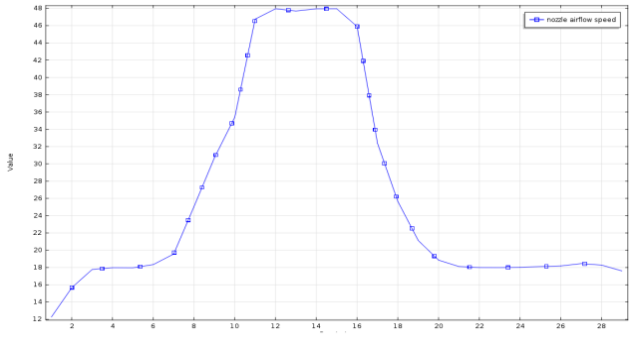

(b)

Fig.4. (a) Nozzle shaped OWC chamber, (b) inflow evolution along the chamber.

2.3 Device structure optimization

The desgin of the OWC air nozzle chamber accumulator inspired from venturi tube principal as shown in the Figure.5 bellow, where *Dch* denotes the tube diameter, *θth* throat expansion angles, *Dth* is the nozzle throat diameter, *Hs1* is the length of the first station submerged on the water, *Hs2* the length of the second station exposed to the external air, *Hth* the length of the throat and *L* the chamber height.

The scale of the simulated model is 1:30 the original sculpture dimensions as shown in the Figure 7, the experimental model is based on the same dimensions in order to validate the collected data and make a comparison between both the calculated and the experimental results. In term of optimization, different cases with various conditions have been done in order to study the effects of the different dimensions as: the throat expansion angles, the length of the throat and the area ratio between the inlets and the throat to improve the performances of OWC Chamber device and maximizing the extracted power from the incident wave. During the study process, two parameters were changed and the others were kept constant to differentiate the effects of each parameter on the conversion ratio of the conversion chamber.

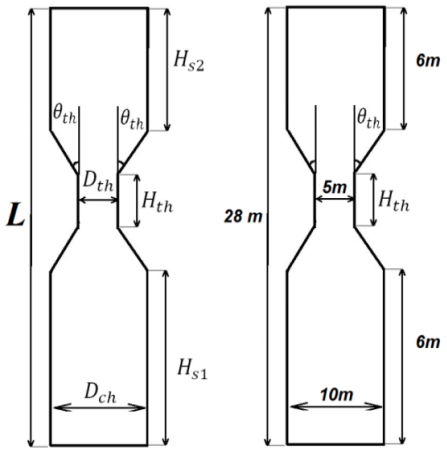

Fig.5. dimensions associated to the venturi tube collector.

Table. 1. Dimentions test conditions for for the OWC chamber collector

Case	***θth*** ***(°)***	**Hsl** **(cm)**	**Hc2** **(cm)**	***Dth*** ***(cm)***	***Dch*** ***(cm)***	***Hth*** ***(cm)***
1	0°	60	60	50	100	130
2	10°	60	60	50	100	120
3	20°	60	60	50	100	110

4	30°	60	60	50	100	100

The standard k-ε model is applied to describe the movement phenomenon of both the water and air dynamic motion, this model is widely applied in the studies of the turbulence and the behaviour of various systems in the engineering researches since it's relatively simple to implement, Leads to stable calculations that converge relatively easily and reasonable predictions for many flows with strong curvature to the flow, or jet flow.Morover, It does perform well for external flow problems around complex geometries.

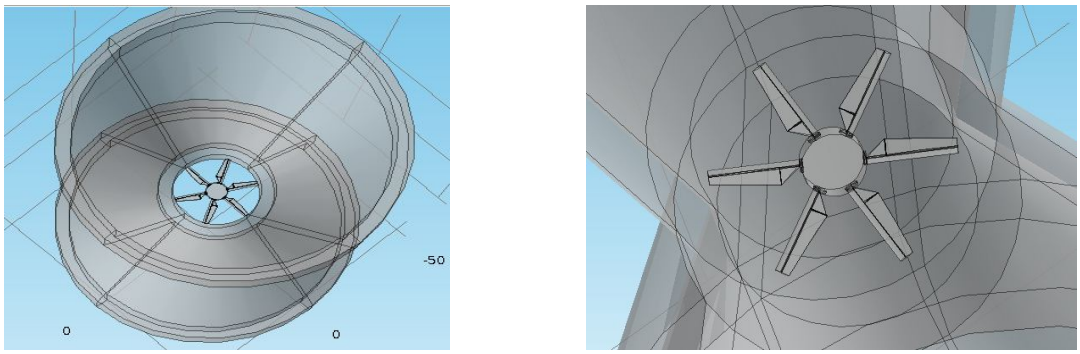

Figure.6. 3D double side orifice structure for the conversion chamber

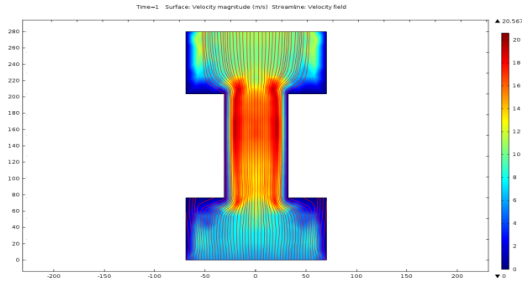

(a)

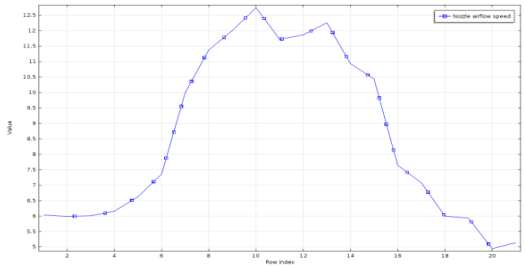

(b)

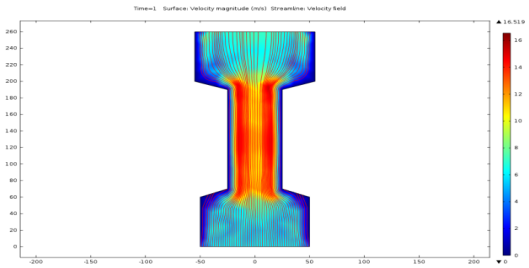

(c)

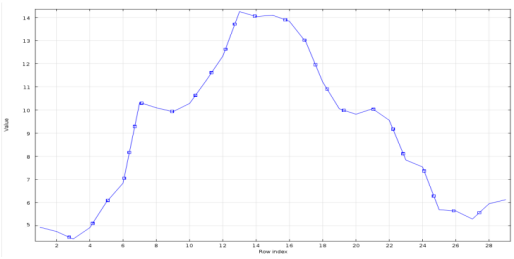

(d)

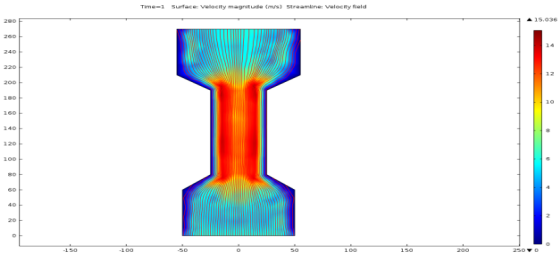

(e)

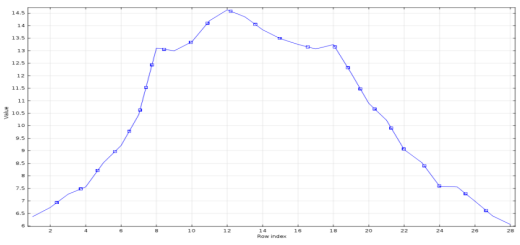

(f)

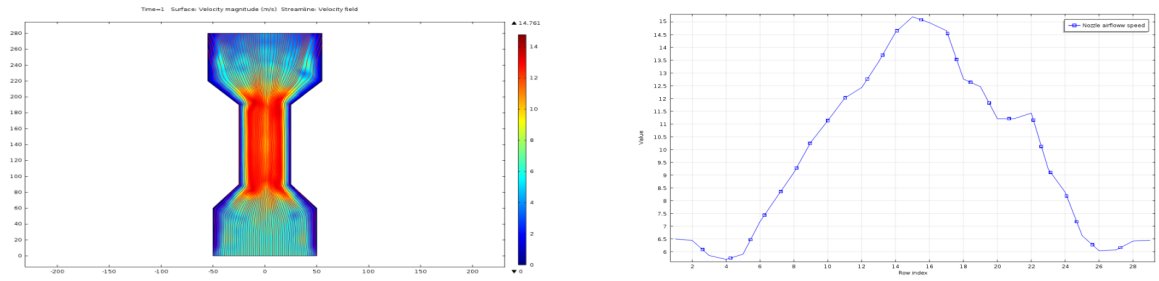

(g) (h)

Fig.7. (a, c, e, g)Airflow velocity along the tube for 0°,10°,20°,30° expansion angles respectively, (b, d, f, h) Airflow streamline for 0°,10°,20°,30° expansion angles respectively.

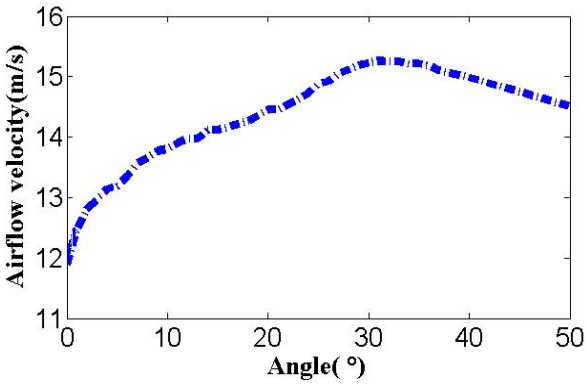

(a)

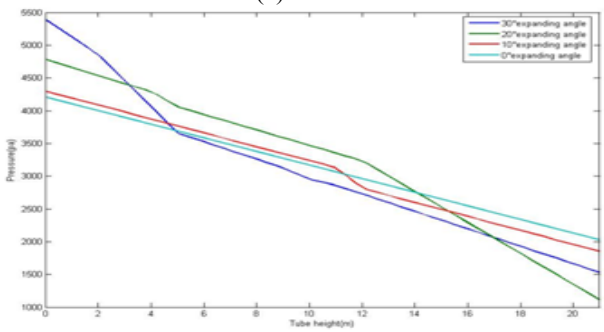

(b)

Fig.8. Airflow velocity versus angle changes graph (a), tube pressure changes versus tube height graph (b).

The results given by the CFD simulation study during the optimization process of the double orifice form shows the existence of an optimum point to reach a high flow rate around the turbine area, the 30° inclination of the throat angle θ allows the structure to reach the highest conversion rate performances.

2.4 Incident wave form and the RWMS method

To study the behaviour of the system including both the structure and the turbine, the incident wave form has a major effect on the study achievement process and the more the model is close to reality the more the system is reliable.

The majority of the studies and the published works take the incident wave on their studies as a sinusoidal wave form or an ISSC (International Ship Structure Congress) spectrum to simplify the model and to give less complexity during the calculation process. However, since the wave form is an irregular wave containing variable parameters which are NOT periodically vary; this affects the obtained results and affects the behaviour of the studied model.

RWMS method (Real Wave Model Simulator) is the issue that has been used by the authors to get a model close to the real wave form instead of using an ordinary sin wave generator. The method based initially on the generation of an irregular waves on the experimental test tank through a mechanical device illustrated on the figures 11(a) and (b), an ultrasonic sensor has been used to get the state of the elevation surface. Then, the data has been stored on an array data form; the regenerated wave was fitted and implemented on the TMS320C7611 board initially. Later, the model has been implemented on Labview software system using RT-FPGA model with Myrio board to be used as a reference for OWC system.

The Figure 12 given bellow illustrates the fitted curve of the captured data for the constructed prototype.

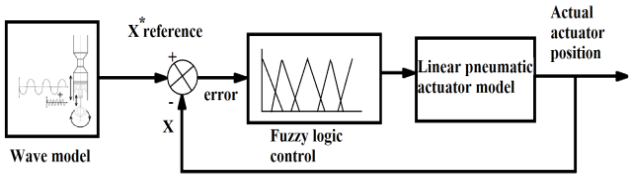

Fig.9. Fuzzy logic based closed loop control for the wave generator device.

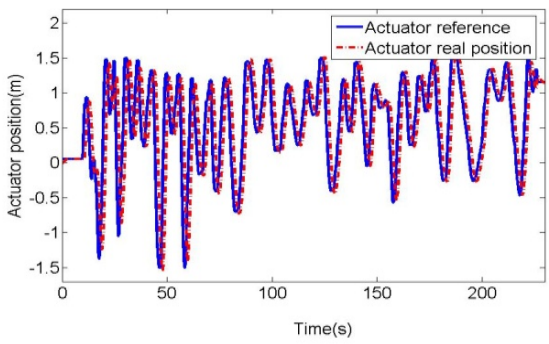

Fig.10. Wave generator model device control test results.

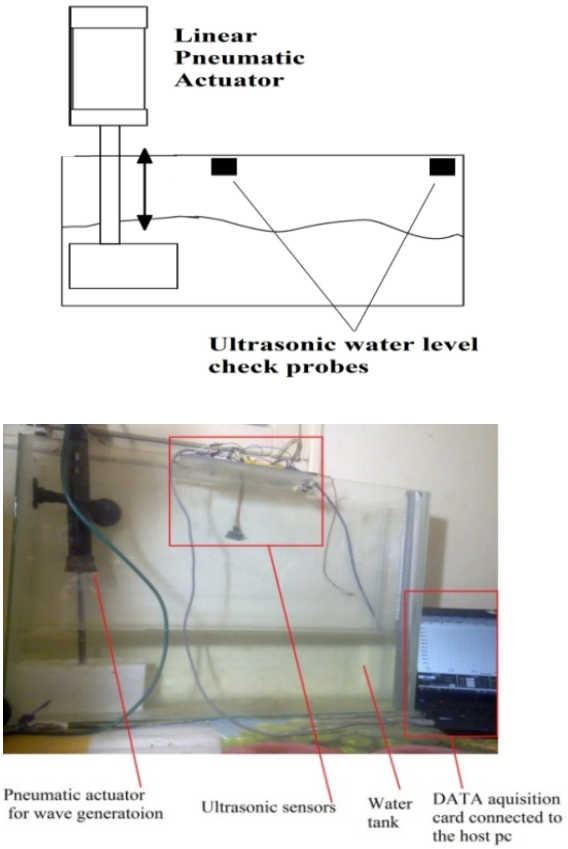

Fig .11. The built prototype for wave form extraction model.

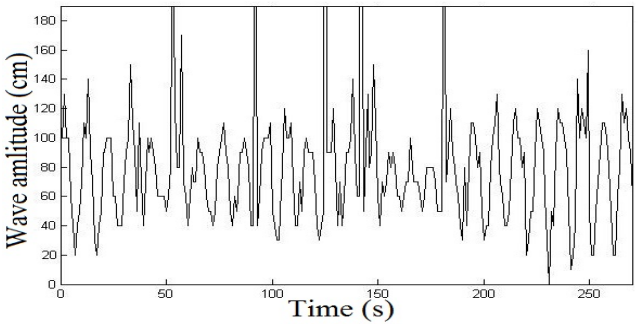

Fig.12. Fitted curve of the lookup table from the captured data on the oscillated water built prototype.

For the experimental part, 10 airflow probes have been placed along the orifice structure, the propagation of the flow throw the chamber to the throttle where the turbine supposed to be installed has been captured during 2787 seconds. The figures below give the experimental results obtained using the RWMS built structure with a data acquisition board connected to a host pc with LABVIEW software working on real time interfacing the data coming from the installed probes.

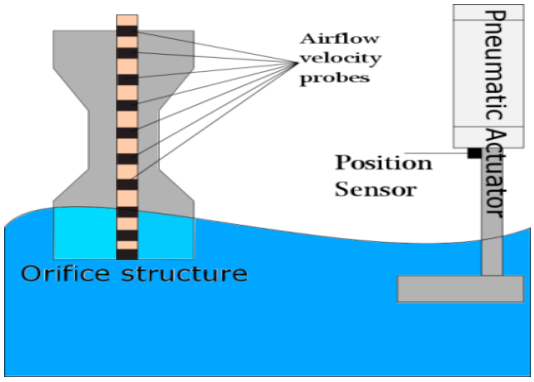

Fig.13. RWMS built system illustration

The graphs below illustrate the data captured from the pneumatic actuator controlled through a fuzzy set closed loop system and the different probes installed on the RWMS simulation device along the orifice chamber structure (Figure 13). The experiment during a real time process execution shows the evolution of the flow velocity for both phases upstream and downstream of the waves upcoming on the compression chamber.

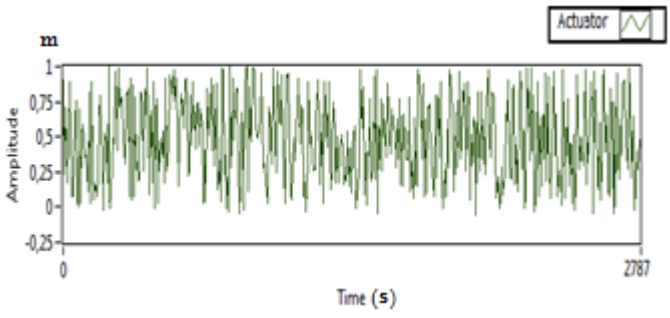

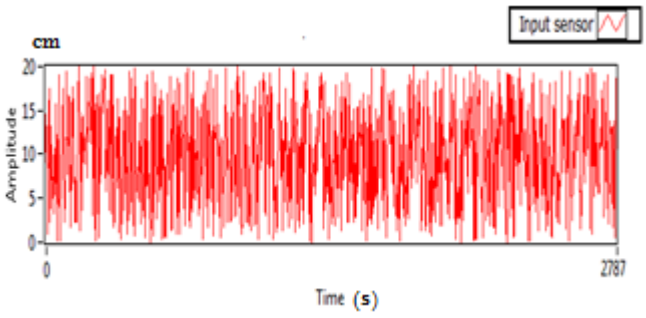

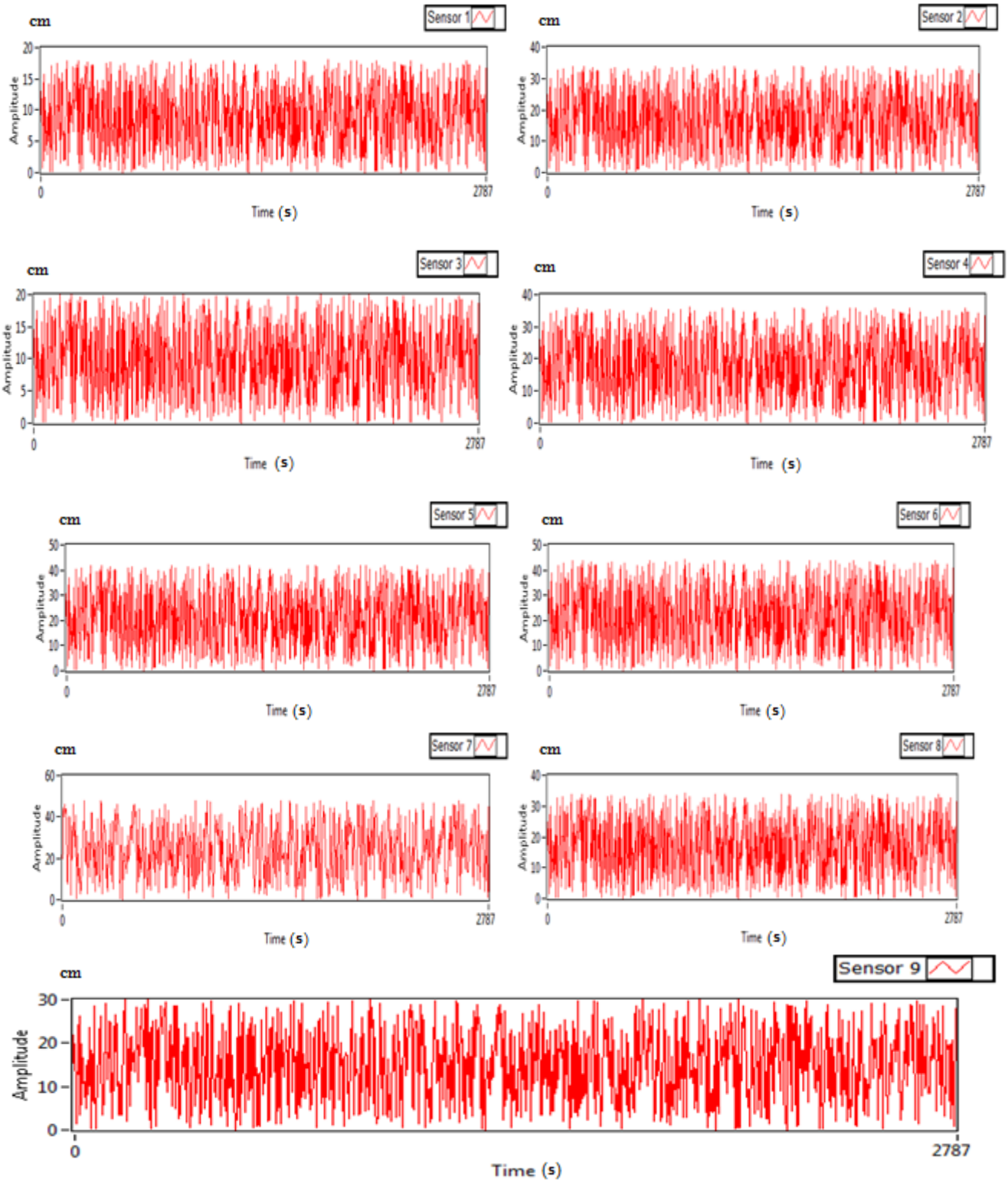

Fig.14. Experimental results for the air flow velocity variation inside the orifice construction model

The evolution of the flow velocity recorded and given above can be summarized within a single curve illustrates the state of airflow velocity on each level along the chamber structure as the figure (15) shows.

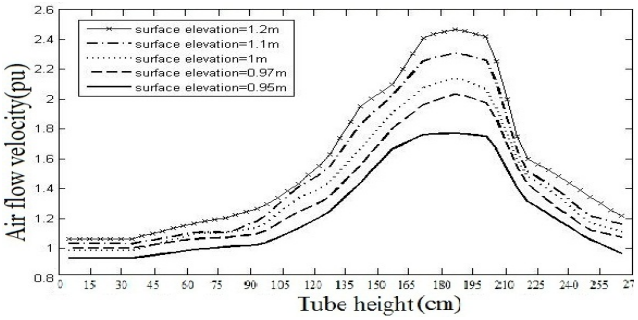

Fig.15. Experimental results airflow velocity for double sided orifice structure related to the surface elevation area.

3. Wind generation system studying

For the design of the wind turbine system, the information about the installation cite is necessary. An installation area has been proposed for the designed system in YEMA GORAIA the BEJAIA coastal region. The yearly forecasted data for the windy region provided by the CNDER (centre national des energies renouvlables) the Algerian national centre for renewable energies of the region are illustrated below.

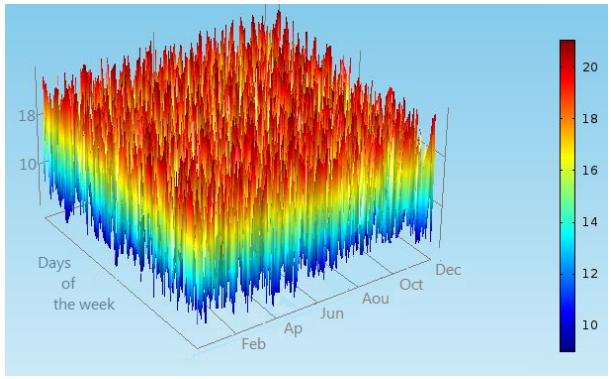

Fig.16. Yearly monthly and daily wind data profile applied for the model study

The modelling of the 5 wind generators for the proposed farm within the desired cite has been done using the CFD study model. By using the data provided and illustrated early, the available wind power around each generator is used during the simulation process of the system. The CFD modelling data results are illustrated on the figures below.

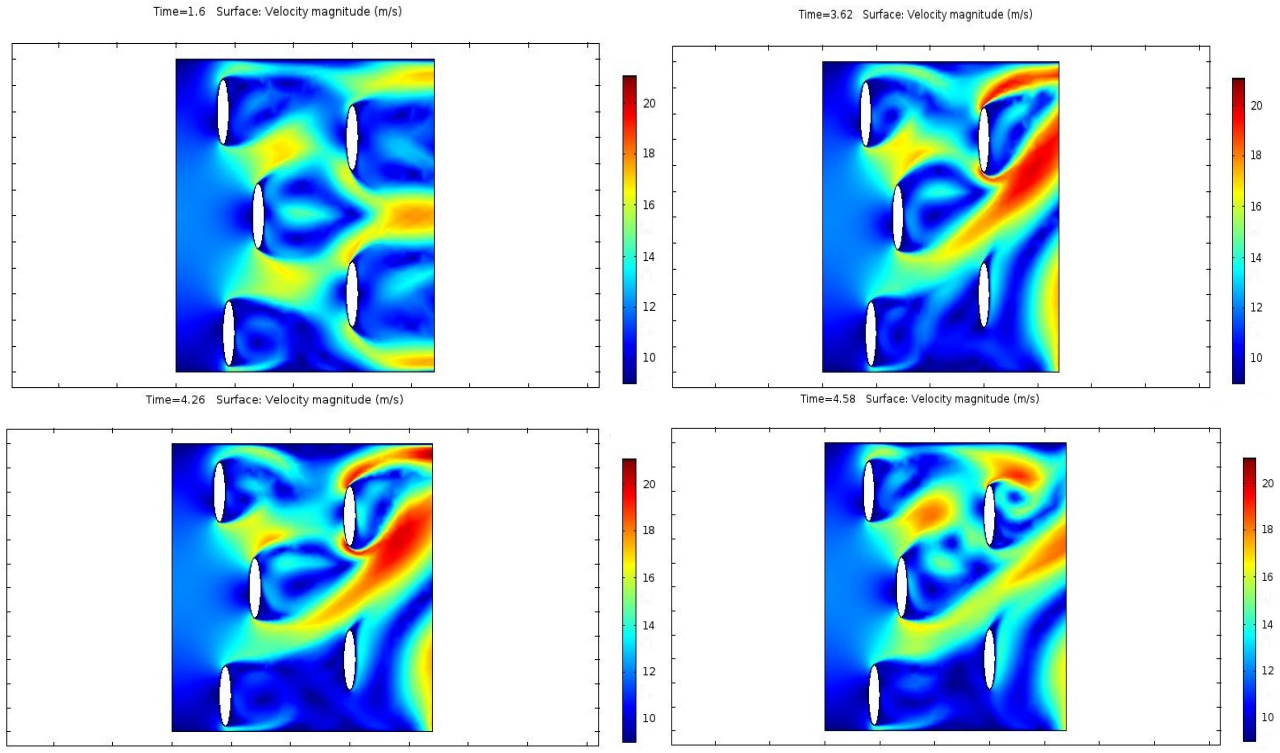

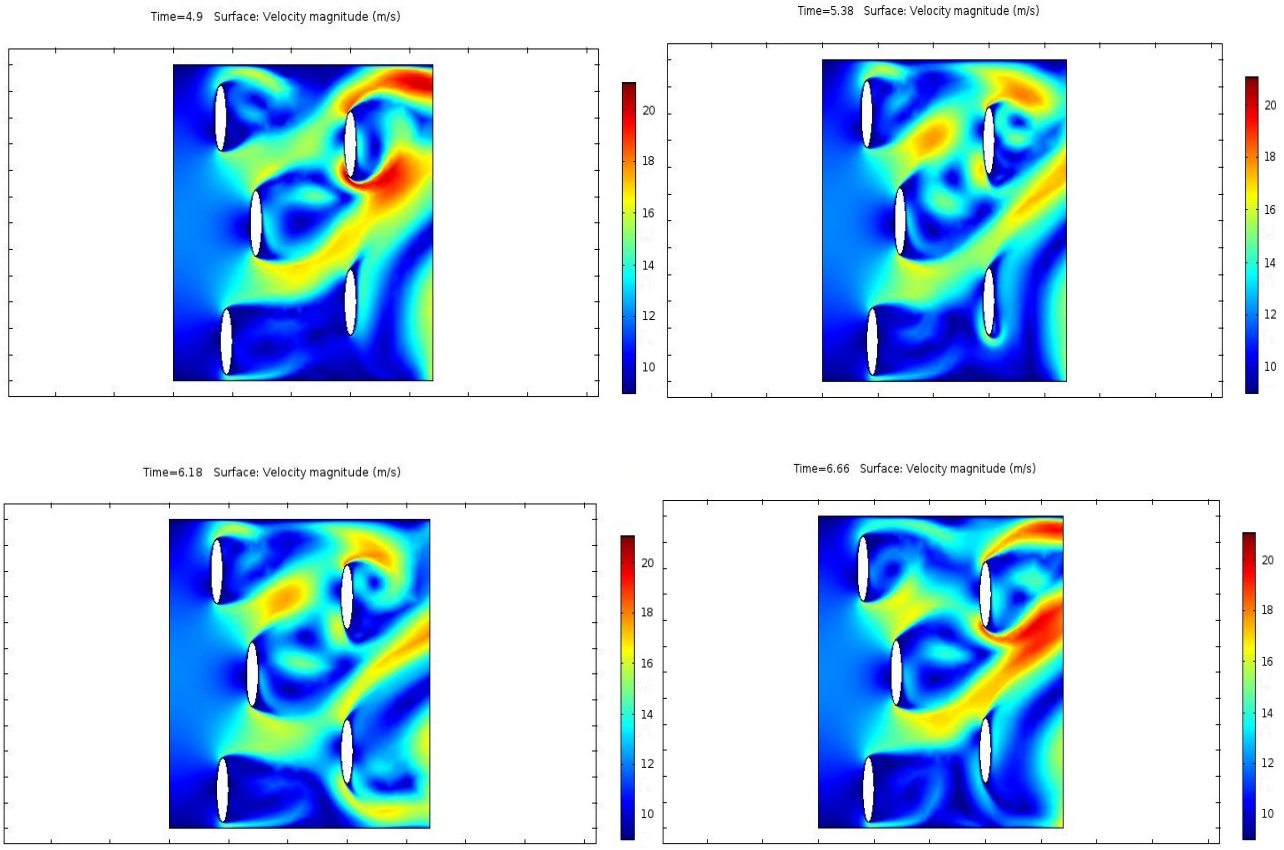

Fig.17. Wind farm air flow dynamics study using CFD simulation around the 5 turbine generators

The wind generators have been arranged with a manner that each generator harvests the maximum energy possible regarding the available surface on the installation cite. The average wind speed around each turbine is shown below.

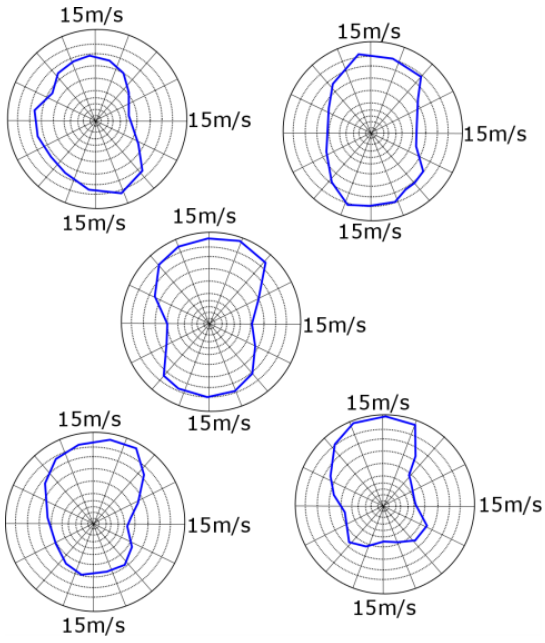

Fig.18. Simulation results for the average Air flow velocity ratio around the 5 wind turbines generators.

4. Solar system and battery storage system for wind energy control feeding and power flow management with DC_DC two phase interleaved boost converter (IBC)

Unidirectional power converters can be very cost effective in these systems, but offshore wind turbines and OWC generators turbines also need power to be supplied when there is no wind in order to feed their controllers. Since, power generated is in the range of megawatt, whereas only tens KW are needed to feed the turbine when it is not in generation mode and to keep control over the pitch and yaw control systems of the turbine. For this purpose, a photovoltaic generator with battery storage system has been integrated within the proposed system, where a part of the generated power is used to cover the control of the wind generator required power. Whereas, the other part is used for the grid feeding and charging the battery storage system parts.

Novel ideas from various studies proposes the uses of the interleaved converter for power control on the multi sources generating systems based on renewable energy systems applications like photovoltaic power system management, cells storage systems, wind generators etc. The different parallel switching topologies proposed for the interleaved converters structures control aim to reduce current stress and maximize its performances [13-14]. Its proved that the interleaved converters offer better input current with a reduced output voltage ripples [11, 12, 15, 16].from this point, the IBC systems are adopted as a base converter units in the hybrid power system management. Parallel two phase switching devices are adopted on this work for system power management generated from the different sources starting from the wind generators, the OWC system, the wind generator control system based on photovoltaic solar generator and the battery storage system. The delivered power on the DC bus is transmitted to the grid through a grid side power converter system. The proposed structure depicted in Figure 19 is basically a parallel connection between boost converters with a common output filter. This structure follows the concept of switching capacitor based voltage multiplier cell. The sequence of operation is analyzed in detail on this work. For this topology, the duty cycle D must be constrained to D>0.382 to ensure the correct behaviour as illustrated on a work presented by Arango et al., 2012 [17]. The operation sequence topology for the converter system are obtained by means of the classical approach summarized on 4 different modes where

Mode1: S2 and D1 ON; S1 and D2 OFF

Mode2: S1 and D2 ON; S2 and D1 OFF

Mode3: S1 ON; S2, D1 and D2 OFF

4.1 Power interleaved converter topology

The figure below shows the power circuit topology for the interleaved converter used for the battery charging system. The main basic idea for the converter is the use of parallel topology of a simple DC-DC boost converter by managing the control pulses between the switches of the two stages.

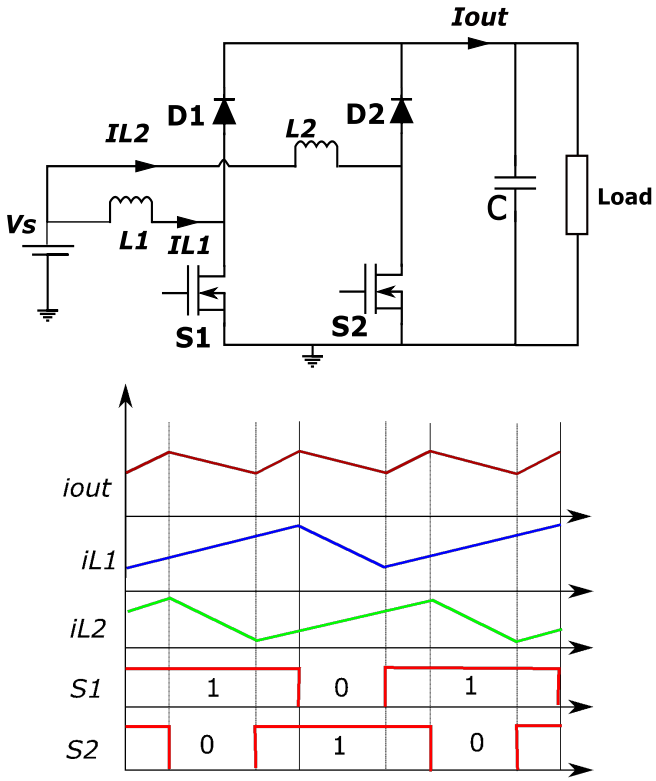

Fig.19. Two phase interleaved converter diagram for DC link voltage control

4.2 Two phase interleaved converter modelling for Battery storage system power management

The differential equations for the different operating modes are illustrated in bellow

Mode1:

$$\frac{di_{l1}}{dt} = -\left(\frac{r_{l1}+r_{s1}}{l1}\right)i_{l1} + \frac{v_s}{l1} \tag{29}$$

$$\frac{di_{l2}}{dt} = \frac{v_s}{l2} - \frac{v_{d2}}{l2} - \frac{Rv_c}{l2(R+r_c)} - i_{l2}\left[\left(r_{l2}+r_{d2}\right) + \frac{Rv_c}{(R+r_c)}\right]\cdot\frac{1}{l2} \tag{30}$$

$$\frac{dv_c}{dt} = i_{l2}\frac{R}{c(R+r_c)} - \frac{v_c}{c(R+r_c)} \tag{31}$$

$$\dot{X} = AX + BU \tag{32}$$

$$X = \begin{bmatrix} i_{l1} \\ i_{l2} \\ v_c \end{bmatrix}, U = \begin{bmatrix} v_s \\ v_{d1} \\ v_{d2} \end{bmatrix} \tag{33}$$

$$A1=\begin{bmatrix} -\left(\frac{r_{l1}+r_{s1}}{l1}\right) & 0 & 0 \\ 0 & -\left[\left(r_{l2}+r_{d2}\right)+\frac{Rv_c}{(R+r_c)}\right].\frac{1}{l2} & -\frac{Rv_c}{l2(R+r_c)} \\ 0 & \frac{R}{c(R+r_c)} & -\frac{1}{c(R+r_c)} \end{bmatrix} \quad (34)$$

$$B1=\begin{bmatrix} \frac{1}{l1} & 0 & 0 \\ \frac{1}{l2} & 0 & -\frac{1}{l2} \\ 0 & 0 & 0 \end{bmatrix} \quad (35)$$

Output equation

$$V_o=\frac{A1.v_c}{R+r_c}+i_{l2}\frac{A1.r_c}{R+r_c}, Y_1=C_1^{\,T}X, C_1^{\,T}=\begin{bmatrix} 0 & \frac{R.r_c}{(R+r_c)} & \frac{R}{(R+r_c)} \end{bmatrix} \quad (36)$$

Mode2:

$$\frac{di_{l1}}{dt}=-\left(\frac{r_{l1}+r_{s1}}{l1}\right)i_{l1}+\frac{v_s}{l1} \quad (37)$$

$$\frac{di_{l2}}{dt}=\frac{v_s}{l2}-i_{l2}\left[\left(r_{l2}+r_{s2}\right)\right].\frac{1}{l2} \quad (38)$$

$$\frac{dv_c}{dt}=\frac{v_c}{c(R+r_c)} \quad (39)$$

$$X=\begin{bmatrix} i_{l1} \\ i_{l2} \\ v_c \end{bmatrix}, U=\begin{bmatrix} v_s \\ v_{d1} \\ v_{d2} \end{bmatrix}, \quad (40)$$

$$A2=\begin{bmatrix} -\left(\frac{r_{l1}+r_{s1}}{l1}\right) & 0 & 0 \\ 0 & -\left[\left(r_{l2}+r_{s2}\right)\right].\frac{1}{l2} & 0 \\ 0 & 0 & -\frac{1}{c(R+r_c)} \end{bmatrix} \quad (41)$$

$$B2=\begin{bmatrix} \frac{1}{l1} & 0 & 0 \\ \frac{1}{l2} & 0 & 0 \\ 0 & 0 & 0 \end{bmatrix} \quad (42)$$

Output equation

$$V_o=\frac{R.v_c}{R+r_c}, Y_2=C_2^{\,T}X, C_2^{\,T}=\begin{bmatrix} 0 & 0 & \frac{R}{(R+r_c)} \end{bmatrix} \quad (43)$$

Mode3:

$$\frac{di_{l1}}{dt}=-\left(\frac{Rv_c+(R+r_c)(r_{l1}+r_{d1})}{R+r_c}\right).\frac{1}{l1}.i_{l1}+\frac{v_s}{l1}-\frac{v_{d1}}{l1}-\frac{Rv_c}{l1(R+r_c)} \quad (44)$$

$$\frac{di_{l2}}{dt}=\frac{v_s}{l2}-i_{l2}\left[\left(r_{l2}+r_{s2}\right)\right].\frac{1}{l2} \quad (45)$$

$$\frac{dv_c}{dt}=i_{l1}\frac{R}{c(R+r_c)}-\frac{v_c}{c(R+r_c)} \quad (46)$$

$$X=\begin{bmatrix} i_{l1} \\ i_{l2} \\ v_c \end{bmatrix}, U=\begin{bmatrix} v_s \\ v_{d1} \\ v_{d2} \end{bmatrix} \quad (47)$$

$$A3=\begin{bmatrix} -\left(\frac{Rv_c+(R+r_c)(r_{l1}+r_{d1})}{R+r_c}\right).\frac{1}{l1} & 0 & \frac{R}{l1(R+r_c)} \\ 0 & -\left[\left(r_{l2}+r_{s2}\right)\right].\frac{1}{l2} & 0 \\ \frac{R}{c(R+r_c)} & 0 & -\frac{1}{c(R+r_c)} \end{bmatrix} \quad (48)$$

$$B3=\begin{bmatrix} \frac{1}{l1} & -\frac{1}{l1} & 0 \\ \frac{1}{l2} & 0 & 0 \\ 0 & 0 & 0 \end{bmatrix} \quad (49)$$

Output equation

$$V_o = \frac{R.r_c}{R+r_c} + i_{l1}\frac{R.r_c}{(R+r_c)}, Y_3 = C_3^T X, C_3^T = \begin{bmatrix} \frac{R.r_c}{R+r_c} & 0 & \frac{R}{(R+r_c)} \end{bmatrix} \quad (50)$$

4.3 Simulation and experimental results for the battery power charging converter system

The simulations of the whole system were carried using MATLAB simulink. The figure (22) shows the output voltage of the converter charging 300V battery cell system from a DC power source.

After simulation the charging system, the model was built and tested. The resulting behaviour is very close to simulation results figure (22). Figures illustrated below show the converter output charging the prototype battery bank for the designed system. During the simulation of the whole wind farm system, the battery behaviour shows a power peak of 27.5 kW. This phenomenon has been taken into consideration during the system calculation and built process. Hence, a 27648 W battery capacity have been installed containing 32 cells unit with 24 V, 36 A and 140Ah each figure(22).

A protection circuit containing: temperture checking , overvoltage protection, overcurrent protection, short circuit protection and battery heat checking have been placed for the safety of the battery storage element.

The protection circuit cover even the interleaved power system protection for the overheat and the short circuit or over load problems.

A second interleaved with parallel connection to the main converter has been placed for emergency inetraction.

The figure bellow (figure.20) illustrates the parallel connection schematic between the two converters to the power source and the load.

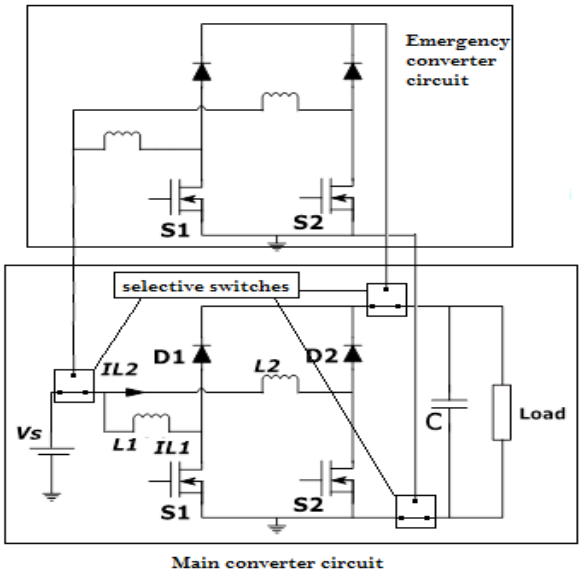

Fig.20. Converter main circuit with emergency converter connection

Fig.21. Lead Acid Battery bank system with the charge protection circuit

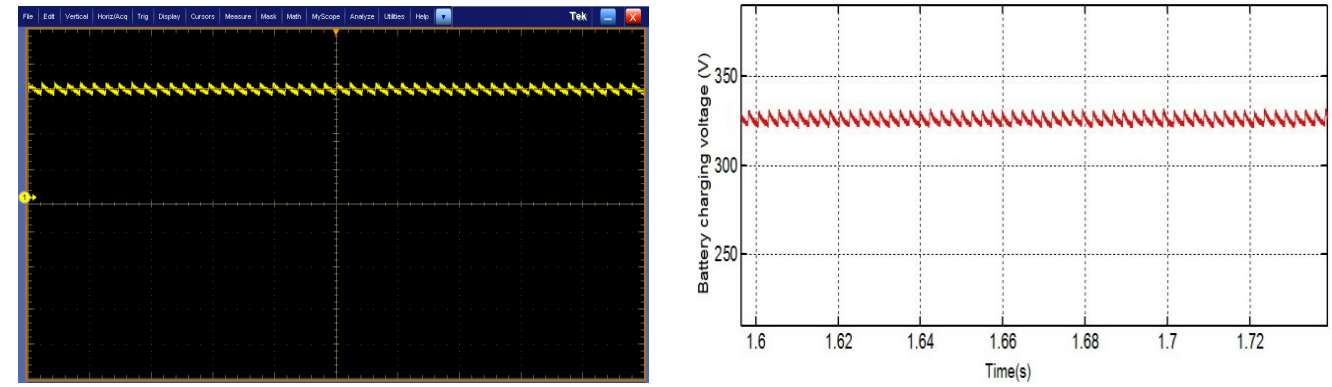

(a)

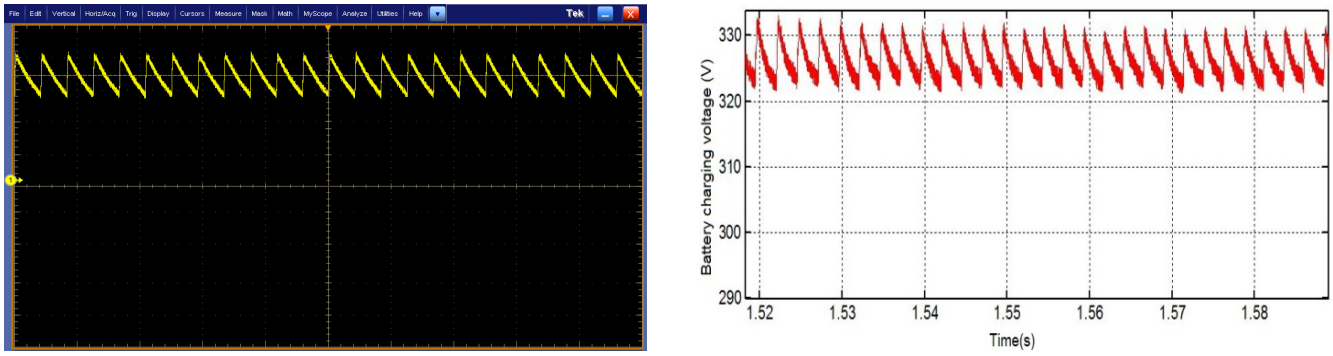

(b)

Fig.22. Simulation and Experimental results for battery charging system with two phase interleaved converter system

5. Full wind farm generation system simulation

Offshore farms can benefit from direct connection of their wind turbines to medium DC distribution lines. The power converter cost can be low if the connection is unidirectional and only diodes are used in the high voltage side, However, the wind turbines require electric power to operate their control electronics and pitch and yaw systems. The below figure (23) illustrates the adopted multi-system generator topology based on DC connection system generation in between the different sources of the farm. Connection structure of the offshore wind turbines and marine energy generators (OWC) to DC distribution lines within the wind farm can reduce the cost of energy. The power management process using the DC system control based on the two phase interleaved controllers for the power flow should handle the full power control through the connection grid.

The illustrated diagram shows an offshore wind farm system conception design for 5 wind generators with 8.5 kW range each has been used. Diode rectifier systems with MPPT control have been adopted for the control of the generators on both sides the wind and the OWC generation systems. The CFD study data obtained and the behaviour of the different structures has been taken into consideration for the whole system simulation process.

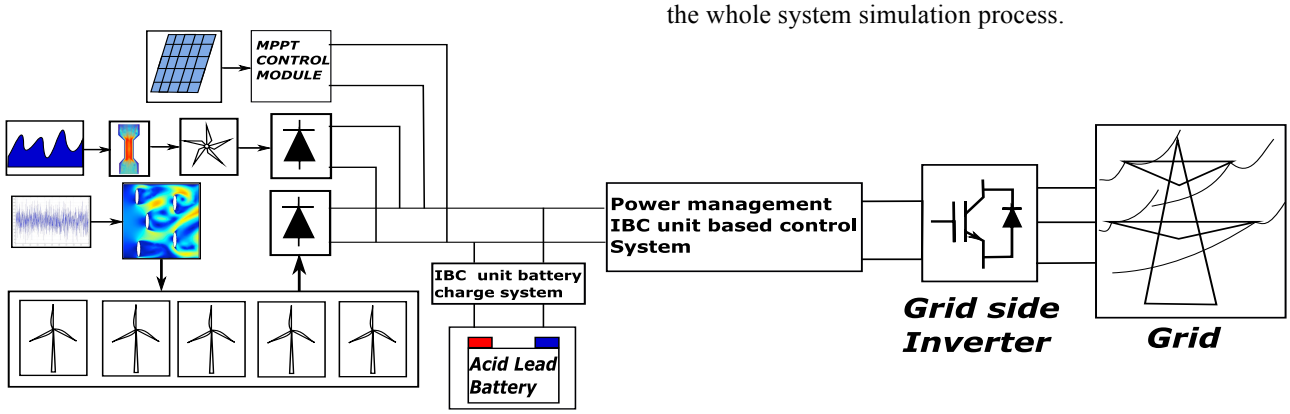

Fig.23. Global diagram for the wind generator system with battery storage and OWC generation system

The simulation results for the full system functionality are illustrated in below.

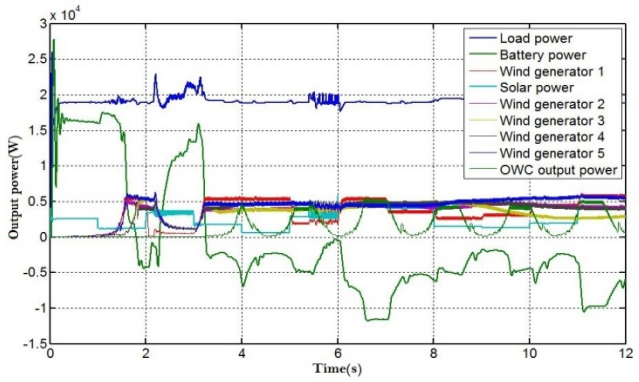

Fig.24. Power output simulation results from the different part of the system

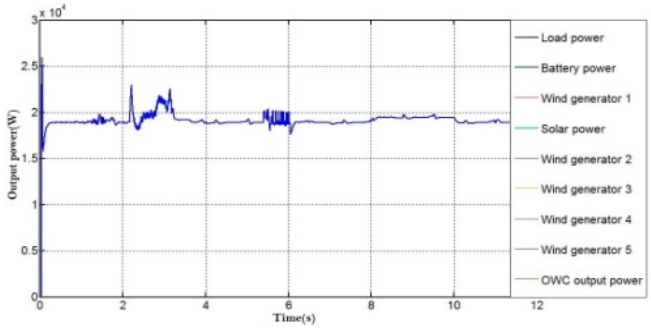

(a)

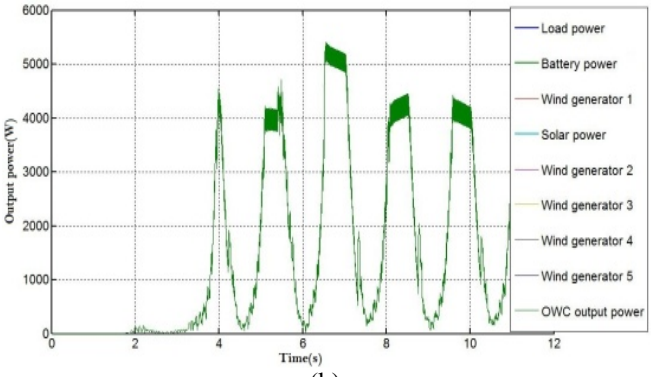

(b)

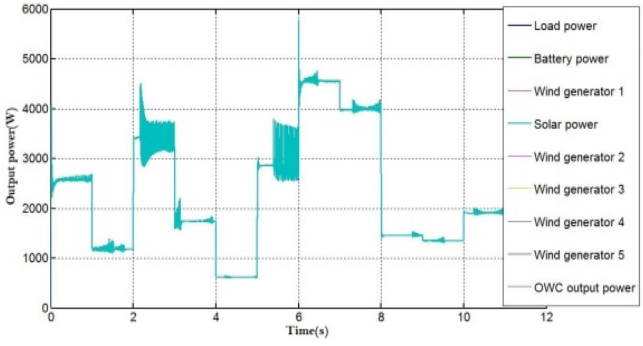

(c)

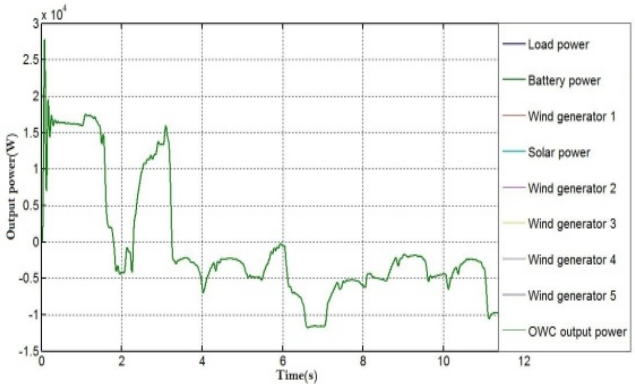

(d)

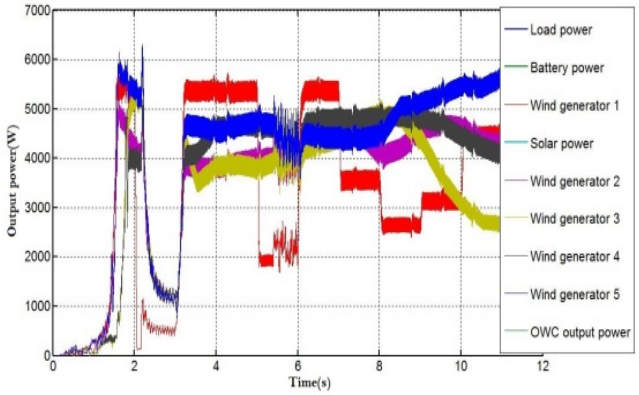

(e)

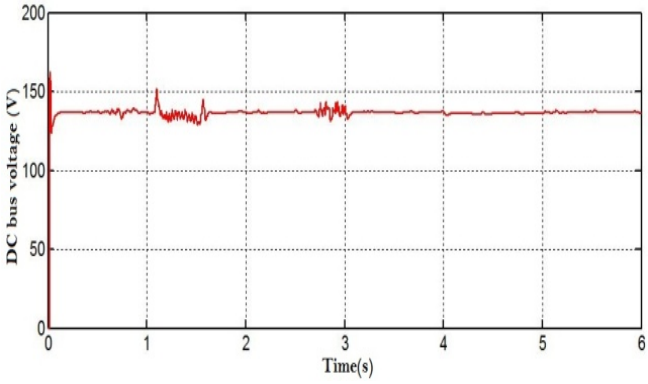

(f)

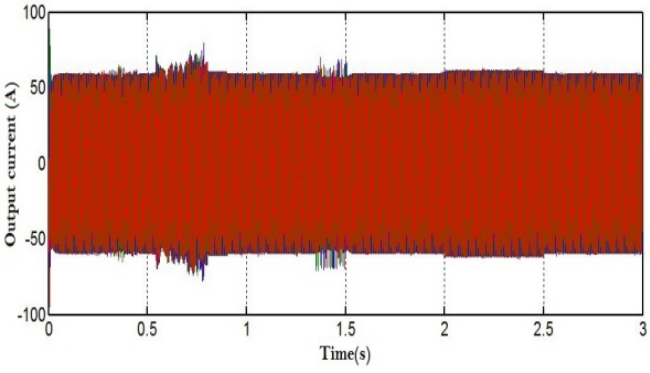

(g)

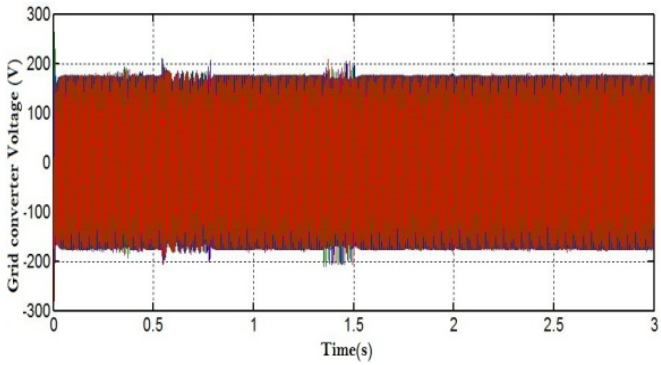

(h)

Fig.25. System simulation results respectively (a) load power, (b) OWC generator output power, (c) solar system output power, (d) battery storage power, (e) wind turbine output power, (f) DC bus voltage, (g) inverter grid side output current system, (h) inverter output voltage system.

Acknowledgements

This material is based on a work supported by the LGEC (laboratoire de génie élèctrique) laboratories, faculty of ELECTRICAL ENGINEERING. Constantine 1 University within the fund for research groups of electrical laboratories of the UNIVERSITY OF CONSTANTINE1 within the current research topic EnR 2015-2030 supported by the Ministry of Mines and Energy (MME) of Algeria.

6. Conclusions

The paper gives the present status of art on a proposed full offshore wind farm generation system using WTGS in conjunction to a double orifice wave energy conversion chamber optimized structure for power lifting process. The characteristics of the wave energy conversion structure have been discussed. The investigation on the model parameters optimization have been proposed for the power rate maximization by CFD and FEM numerical simulation and experimentally validated using a novel method proposed for the first time by the authors called **RWMS** method (Real Wave Model Simulator) as an issue to get a model close to the real wave form instead of using an ordinary sin wave generator generally used on the published works**.** The **s**tudy results show that the OWC conversion compression chamber reach the maximum conversion rate around the a central installed turbine model for an angle around the 30° optimizing the different parameters and performing the different characteristics for the double orifice proposed model. A lead acid battery bank storage system based on two phase interleaved charging system has been simulated and experimentally validated. For the wind generator and the orifice turbines control, a full controlled solar system has been used for this purpose. The prototype building process is under construction for the final installation as a first prototype of its kind on the desired area.

References

[1] Uk department of trade and industry “sustainable Energy route maps:wave energy” http://www.berr.gov.uk/files/file27084.

[2] K. Y. Hong, S. H. Shin, D. C. Hong, H. S. Choi and S. W. Hong. Effectsof shape parameters of OWC chamber in wave energy absorption. *Proc* 17th Int Offshore and Polar EngConf, Lisbon, Portugal, ISOPE, 2007.Vol. 1, pp. 428-433.

[3] Y. G. You, Hydrodynamic analysis on wave power devices in near shore zones. *Journal of Hydrodynamics*, Ser. B 1993. Vol. 5, pp. 42-54.

[4] T .Heath, T .Whittaker, C. B. Boake, “The design, construction and operation of the LIMPET wave energy converter (Islay Scotland)”. In: The fourth European Wind Energy Conference. Aalborg, Denmark. 2000, pp.78~83.

[5] N.A. Brown and D.A. Innis, “Offshore Floating Ocean Energy System,” *US Patent No.8,446,030 B2,*2013

[6] F .Johnson, J .Chudley, Y. M .Dai, “Prolongation of the Deployment and Monitoring of a Multiple Oscillating Water Column Wave Energy Converter”.The University of Plymouth, UK.2003, pp.23~32.

[7] Basque Energy Board (EVE). [Online]. Available: http://www.eve.es/ web/Energias-Renovables/Energia-marina.aspx?lang=en-GB.

[8] Y.Torre-Enciso,”Mutriku Wave Power Plant:From conception to reality,”Eur.Fed. of Region.Energy and Environ.Agencies(FEDARENE),Brussels, Belgium,Dec.2009.

[9] M. Delucchi, “Wind, water and solar power for the world,” *IEEE Spectrum Online*, Sep. 2011.

[10] R. G. Alcon, B W. Ceattie,” Observations of time domain dataon the Wells turbine in the islay wave power plant”,.In:Proceedings of the eighth Internaional Offshore and polar Engineering Conferences.Montrial, Canada:International Society of Offshore and Polar Engineers,1988. pp.12~18.

[11] N. Subramanian, P. Prasanth, R Srinivasan, Dr.R.Seyezhai and R RSubesh, “ Review of uncoupled, coupled inductor and RCN based two-phase interleaved boost converter for photo-voltage applications” International Journal of Electronics, Electrical and Computational System IJEECS., ISSN 2348-117X Volume 3, Issue 3, May 2014, pp.45-52.

[12] Ajit T. N, “Two Stage Interleaved Boost Converter Design and Simulation in CCM and DCM”, India International Journal of Engineering Research & Technology (IJERT) Vol.3Issue7, July-2014, pp847-851.

[13] B. Khasawneh, M.Sabra, M.A.. Zohdy, “Paralleled DC-DC Power Converters Sliding Mode Control with Dual Stages Design”, Journal of Power and Energy Engineering, 2014, 2,1-10 (February 2014),pp 1-10.

[14] S .Mazumder, .K., A.H..Nayfeh, , Borojevic, A, “Robust control of parallel DC-DC buck converters by combining integral-variable- structure and multiple-sliding-surface control schemes”, IEEE T POWER ELECTR, (Volume:17 , Issue:3),May 2002, pp. 428 – 437.

[15] Tin-Ho Li, R,Ho, C.N.M, "An Active Snubber Cell for N-Phase Interleaved DC-DC Converters", International Electronics and Application Conference and Exposition (PEAC), Nov 2014, pp.953 – 958.

[16] L .Dinca, J.-I Corcau, , E .Ureche, "Optimization of a dc to dc boost converter using interleaved command technique", *9th International Symposium Advanced Topics in Electrical Engineering (ATEE)*, 2015 May2015, pp. 644 – 649.

[17] E. I. Arango Zuluaga , C. A. RamosPaja and A. J. SaavedraMontes,"Modeling of asymmetrical boost converters ",Ingeniería e Investigación, Vol 34, No 1 , 2014.